

---

# Informed Correctors for Discrete Diffusion Models

---

Yixiu Zhao<sup>1,2</sup> Jiaxin Shi<sup>3</sup> Feng Chen<sup>2</sup> Shaul Druckmann<sup>1,4</sup> Lester Mackey<sup>5</sup> Scott Linderman<sup>1,6</sup>

## Abstract

Discrete diffusion has emerged as a powerful framework for generative modeling in discrete domains, yet efficiently sampling from these models remains challenging. Existing sampling strategies often struggle to balance computation and sample quality when the number of sampling steps is reduced, even when the model has learned the data distribution well. To address these limitations, we propose a predictor-corrector sampling scheme where the corrector is informed by the diffusion model to more reliably counter the accumulating approximation errors. To further enhance the effectiveness of our informed corrector, we introduce complementary architectural modifications based on hollow transformers and a simple tailored training objective that leverages more training signal. We use a synthetic example to illustrate the failure modes of existing samplers and show how informed correctors alleviate these problems. On tokenized ImageNet  $256 \times 256$ , this approach consistently produces superior samples with fewer steps, achieving improved FID scores for discrete diffusion models. These results underscore the potential of informed correctors for fast and high-fidelity generation using discrete diffusion.

## 1. Introduction

Denosing diffusion models are powerful generative models for high-dimensional data (Sohl-Dickstein et al., 2015; Song & Ermon, 2019; Ho et al., 2020). The central idea of diffusion models is to gradually corrupt data into noise using a “noising” or “forward” process and then to train a parameterized model (usually a deep neural network) to learn its time

reversal, commonly known as the “denoising” or “backward” process. In continuous domains like image generation, the forward process is usually defined by gradual injection of Gaussian noise and scaling that transform the data distribution into a standard normal. The backward process is then approximated by learning the gradient of the log density (also known as the “score function”) of the marginal distribution. To draw samples from a trained model, one first generates Gaussian noise and then simulates the backward process using the score information. Diffusion generative models are currently the dominant framework for image generation, and they can generate high-resolution images with stunning details given prompts from a user (Ramesh et al., 2021; Rombach et al., 2022).

Given the success of diffusion models in continuous settings, recent work has explored diffusion modeling in discrete domains (Hooeboom et al., 2021b; Song et al., 2020; Austin et al., 2021; Campbell et al., 2022; Santos et al., 2023; Zheng et al., 2023; Benton et al., 2024; Lou et al., 2023; Shi et al., 2024). Discrete diffusion models can be applied to language (Lou et al., 2023), protein sequences (Watson et al., 2023; Alamdari et al., 2023), graphs (Vignac et al., 2023), and more. Notably, Campbell et al. (2022) developed a general framework for discrete denoising diffusion in continuous time. They formulated the forward and backward processes as continuous time Markov chains (CTMCs), and they learned to predict the distribution over denoised data via an evidence lower bound (ELBO) objective. Concurrent work by Shi et al. (2024); Sahoo et al. (2024) and Ou et al. (2024) focused on discrete diffusion with the absorbing state forward process (a.k.a., masked discrete diffusion), deriving a simple formulation of the ELBO that reduces to a weighted cross-entropy. Shi et al. (2024) also noted that this simple objective provides a unifying perspective to previous works (Campbell et al., 2022; Lou et al., 2023; Benton et al., 2024), all of which are parameterizations and modifications of the same ELBO objective.

Despite the conceptual progress on discrete diffusion, many challenges in implementation still limit the effectiveness of these models. One major challenge lies in the trade-off between efficiency and accuracy in simulating the continuous-time backward process. Song et al. (2021) proposed using approximate MCMC correctors to fix the discretization error in simulating the backward process. Campbell et al. (2022)

<sup>1</sup>Wu Tsai Neurosciences Institute, Stanford University <sup>2</sup>Applied Physics Department, Stanford University <sup>3</sup>Google DeepMind <sup>4</sup>Department of Neurobiology, Department of Psychiatry and Behavioral Sciences, Department of Electrical Engineering, Stanford University <sup>5</sup>Microsoft Research New England <sup>6</sup>Department of Statistics, Stanford University. Correspondence to: Yixiu Zhao <yixiu@stanford.edu>.

extended the predictor-corrector sampling to discrete diffusion models and discovered that the corrector steps significantly impact generative performance. In practice however, a clear understanding of how corrector steps contribute to sample quality is still missing, and recent works (Lou et al., 2023; Shi et al., 2024; Ou et al., 2024; Sahoo et al., 2024) still use predictor-only samplers for generation.

We show that predictor-corrector schemes can be improved by leveraging different sampling methods. Analyzing the forward-backward corrector used by Campbell et al. (2022), we identify its failure mode in masked diffusion and illustrate it with a simple Markov chain modeling task. To address this shortcoming:

1. We propose the informed corrector — an alternative corrector scheme inspired by adaptive Gibbs sampling that fixes the issues of the forward-backward corrector and explicitly targets low-probability dimensions.
2. We propose an accompanying training strategy that leverages the hollow transformer architecture (Sun et al., 2022). Specifically, we propose an ELBO objective based on weighted cross-entropy that provides a stronger training signal.

Sampling with the informed corrector drastically decreases error rate in our synthetic example. On tokenized ImageNet  $256 \times 256$ , we show that the informed corrector, together with our innovations yield diverse, high quality samples competitive with existing diffusion models, using a fraction of the parameters and far fewer model evaluations.

## 2. Background

### 2.1. Continuous-Time Discrete Diffusion Models

Consider a data vector  $x_0 \in \mathcal{S}^D$  sampled from a data distribution  $p_{\text{data}}$ , where  $\mathcal{S}$  is the base space and  $D$  is the dimension or sequence length. Denoising diffusion models (Sohl-Dickstein et al., 2015; Song & Ermon, 2019; Ho et al., 2020; Song et al., 2021) model this unknown data distribution by progressively adding noise to data samples until their distribution converges to a simple target, such as a uniform distribution. Then, a deep neural network is trained to invert this process and remove the noise. This reverse process forms a generative model from which new samples can be drawn. The noising and generative processes are also called the *forward* and *backward* processes, respectively. We will adopt this convention for the rest of the paper.

Continuous-time diffusion models define a forward process with noising distribution  $q_t(x_t|x_0)$  and marginals  $q_t(x_t) = \int q_t(x_t|x_0)q_0(x_0)dx_0$ , with  $q_0 = p_{\text{data}}$  and limiting distribution  $q_T \approx \pi$ . The forward process is designed so that  $\pi$  is simple. Then, a parameterized process with marginals  $p_t^\theta$

is learned to match the true backward process.

When the data is discrete (e.g., text, protein sequences, neural spike counts), the base space becomes a ‘‘vocabulary set’’  $\mathcal{S} = \{1, \dots, S\}$  with size  $S$ , and the forward-process can be described with a continuous-time Markov chain (CTMC) with initial distribution  $q_0$  and transition rate matrix  $R_t \in \mathbb{R}^{\mathcal{S}^D \times \mathcal{S}^D}$ . The off-diagonal terms  $R_t(x, y)$ ,  $x \neq y$  of the matrix represent the rate of state  $x$  transitioning to state  $y$  at time  $t$ , and the diagonals  $R_t(x, x)$  are defined as the negative sum of all other elements in the same row:  $R_t(x, x) = -\sum_{y \neq x} R_t(x, y)$ . Under the assumption that  $R_s$  and  $R_t$  commute for all  $s$  and  $t$ , the finite-time transition probabilities satisfy

$$\begin{aligned} q_{t+\Delta t|t}(y|x) &= \left[ \exp \left\{ \int_t^{t+\Delta t} R_s ds \right\} \right] (x, y) \\ &= I(x, y) + R_t(x, y)\Delta t + o(\Delta t), \end{aligned}$$

where  $I$  represents the identity matrix, and in the square brackets we compute a matrix exponential. The time reversal of this CTMC is also a CTMC, and its transition rate is,

$$\begin{aligned} \tilde{R}_t(y, x) &= R_t(x, y) \frac{q_t(x)}{q_t(y)} \\ &= R_t(x, y) \sum_{x_0} \frac{q_{t|0}(x|x_0)}{q_{t|0}(y|x_0)} q_{0|t}(x_0|y). \end{aligned} \quad (1)$$

Campbell et al. (2022) approximated the backward rate by learning a parameterized denoising model  $p_{0|t}^\theta(x_0|y) \approx q_{0|t}(x_0|y)$ . Alternatively, Meng et al. (2022) and Lou et al. (2023) observed that the ratio  $s_t(y)_x \triangleq q_t(x)/q_t(y)$  plays a similar role as the continuous score function  $\nabla \log q_t(y)$ , up to an additive constant. Therefore, they proposed to learn an approximate score function instead,  $s_t^\theta(y)$ .

The training objective is a negative evidence lower bound (ELBO), which is a function of the approximate backward rate  $\tilde{R}_t^\theta(y, x) = R_t(x, y)s_t^\theta(y)_x$ :

$$\begin{aligned} \mathcal{L}(\theta, x_0) &= \int_0^T \mathbb{E}_{q_{t|0}(y|x_0)} \left[ \sum_{x \neq y} \left\{ \tilde{R}_t^\theta(y, x) \right. \right. \\ &\quad \left. \left. - R_t(x, y) \frac{q_{t|0}(x|x_0)}{q_{t|0}(y|x_0)} \log(\tilde{R}_t^\theta(y, x)) \right\} \right] dt + C, \end{aligned} \quad (2)$$

where  $C$  is a constant independent of  $\theta$ . This is the standard ELBO objective for training continuous time discrete diffusion models.

Given the intractable sums over the exponentially large state space  $\mathcal{S}^D$  above, it is natural to constrain the forward process to be a composition of identical independent processes

on each dimension, where the rate over the entire state  $R_t$  can be written as

$$R_t(x, y) = \beta(t) \sum_{d=1}^D R_b(x^d, y^d) \mathbb{1}_{\{x^d=y^d\}} \quad (3)$$

for a base rate matrix  $R_b \in \mathbb{R}^{S \times S}$ , absorbing the time dependence into the scalar coefficient  $\beta(t)$ . With this factorization of the forward rate, the backward rates are also factorized, but now with a different time-dependent rate  $\tilde{R}_t^d$  for each dimension  $d$ . This means that the objective in (2) can be decomposed nicely into a sum over dimensions, as detailed by Campbell et al. (2022).

## 2.2. Absorbing Discrete Diffusion

For generic discrete data, two forward processes are most commonly used: the uniform process and the absorbing state process. We focus on the absorbing state process in this paper, for which the base rate matrix for each dimension can be written as

$$R_b^{\text{absorb}}(x^d, y^d) = \begin{cases} 1 & y^d = \text{MASK}, x^d \neq \text{MASK} \\ -1 & y^d = x^d, x^d \neq \text{MASK} \\ 0 & \text{otherwise,} \end{cases} \quad (4)$$

where we augment the vocabulary set  $\mathcal{S}$  by introducing the MASK token, which represents the absorbing state. The absorbing state diffusion is important to consider because it is very commonly used to model sequence data without ordinal structure (e.g., text and protein sequences). It is also intimately connected to masked language models (Austin et al., 2021; Devlin et al., 2018; Hoogeboom et al., 2021a).

We use special notation for the absorbing state process. For a sequence  $x \in \{\text{MASK}, 1, \dots, S\}^D$ , we use the mask operator  $y = M^d(x)$  to denote the sequence obtained by changing the  $d^{\text{th}}$  component of  $x$  to MASK. Finally, we denote the masked indices of  $x$  by  $\mathcal{M}(x) \equiv \{d : x^d = \text{MASK}\}$ . The set of non-mask indices is the complement,  $\overline{\mathcal{M}}(x)$ .

Recently, Shi et al. (2024) introduced the MD4 diffusion model, which outperformed previous discrete diffusion models on both text and pixel-level image generation benchmarks. Furthermore, they noted that several continuous time denoising diffusion objectives (including (2)) are mathematically equivalent and can be greatly simplified in the case of masked diffusion. The simplified MD4 loss is:

$$\mathcal{L}_{\mathcal{M}}(\theta, x_0) \triangleq \int_0^T \mathbb{E}_{q_{t|0}(x|x_0)} \left[ \frac{\alpha'_t}{1 - \alpha_t} \sum_{d \in \mathcal{M}(x)} \log p_{0|t}^\theta(x^d | x) \right] dt, \quad (5)$$

where  $\alpha_t \triangleq \exp\left(-\int_0^t \beta(s) ds\right)$  is the survival probability of the token at each position and  $\alpha'_t$  indicates its time

derivative. We denote this loss as  $\mathcal{L}_{\mathcal{M}}$  since it sums over the masked dimensions. As we will show later, this loss has a counterpart,  $\mathcal{L}_{\overline{\mathcal{M}}}$ , that can be combined with the MD4 loss to yield better results for training our diffusion model.

## 2.3. Sampling From the Backward Process

Campbell et al. (2022) proposed to use tau-leaping, an approximate sampling method that allows simultaneous updates to multiple dimensions for a single model evaluation. Tau-leaping assumes that the backward process transition rate is constant between  $[t - \tau, t)$ , regardless of whether states change during that interval. Under this assumption, the number of transitions in the interval is a Poisson random variable, and several transition events can be applied simultaneously.

Leveraging the structure of masked diffusion, MD4 (Shi et al., 2024) used a simpler approach. Instead of trying to approximate the continuous time process, Shi et al. (2024) directly sampled from the finite-time conditional distribution  $q_{t-\Delta t|t}(\cdot | x_t)$ . They call this approach ancestral sampling.

**Corrector steps.** Both the above approaches treat the one-step backward update as independent across dimensions, which accumulates simulation errors over the course of the backward process. To combat this problem, additional corrector steps can be used to ensure the marginal distribution of samples  $x_t$  at time  $t$  matches  $q_t$ . Campbell et al. (2022) show that a corrector process with rates,

$$R_t^c(x, y) = R_t(x, y) + \tilde{R}_t(x, y) \quad (6)$$

leaves the stationary distribution  $q_t$  invariant. In practice, one must use the learned backward rates  $\tilde{R}_t^\theta$  as an approximation for the true backward rates  $\tilde{R}_t$ . This can be thought of as an ‘‘uninformed’’ corrector, as it is simply a summation of the forward and backward rates, neither of which explicitly targets problematic tokens in the masked diffusion setting. Nevertheless, Campbell et al. (2022) show that this uninformed corrector increases sample quality in practice.

**Correcting for the absorbing diffusion.** The necessity of corrector steps is particularly apparent when tau-leaping is used in conjunction with an absorbing forward process. In the reversal of the absorbing process, only transitions from the absorbing state to other states are allowed, which is reflected by the structure of  $\tilde{R}_t$ . Thus, once a token has been generated, it cannot be erased or changed, rendering it impossible for the predictor to fix its own errors. Forward-backward corrector steps mitigate this issue by introducing the forward term  $R_t$ , allowing transitions in the forward direction, resulting in generated tokens being ‘‘masked out’’ again with uniform probability.

Though forward-backward corrector steps solve the issue in

theory, they are far from optimal in practice. The steps can only correct mistakes by masking tokens at random. Ideally, we would like the corrector to make informed transitions based on which states are more likely under the model. This observation motivates us to find a better alternative to the forward-backward corrector.

### 3. Methods

Due to the rigid nature of masked diffusion, generation errors from applying several predictor steps at once may persist throughout the sampling process, potentially affecting model predictions in all future steps. In theory, this compounding error problem can be alleviated via corrector steps. However, existing corrector schemes for discrete diffusion either do not have a way to find errors or require training extra models (Lezama et al., 2022), incurring extra computational costs and increased parameter count. To tackle this issue, we design a corrector scheme that uses the model to inform which tokens to correct, prioritizing tokens that have lower likelihood. We then propose HollowDiff, a combination of improved architecture and training objective to enable the efficient use of this informed corrector. We describe these methods in detail below.

#### 3.1. Informed Correctors

To design a corrector scheme for our sampler, we first identify a Markov chain that has the marginal distribution  $q_t$  as a stationary distribution. For discrete distributions, a straightforward option is to use Gibbs sampling,<sup>1</sup> i.e., we iteratively select an index from  $d = 1, \dots, D$  and resample the  $d$ -th dimension according to the conditional distribution

$$x^d \sim q_t(\cdot | x^{\setminus d}). \quad (7)$$

There are two common ways of selecting the index  $d$ , known as systematic scan and random scan. Systematic scan enumerates the dimensions following a fixed permutation, whereas random scan selects the dimensions uniformly at each resampling step. In both cases, it can take many steps for the Markov chain to “correct” a simulation error in one of the dimensions.

**Informed selection.** To improve efficiency, we use an adaptive random-scan Gibbs sampler with a non-uniform selection distribution (Levine & Casella, 2006; Levine et al., 2005; Łatuszyński et al., 2013; Mitliagkas & Mackey, 2017). We choose this distribution so that the corrector prioritizes updating those dimensions that are more likely to have sim-

<sup>1</sup>Other Markov chains could be employed instead. For example, the forward-backward corrector proposed by Campbell et al. (2022) leverages a birth-death process that has  $q_t$  as the stationary distribution. We also tested locally-balanced Markov processes (Zanella, 2019), but their performance was inferior to Gibbs.

ulation errors. Specifically, we define the confidence score,  $c_d \triangleq \log q_t(x^d | x^{\setminus d})$ , the log-probability of the  $d$ -th dimension of the current sample given all other dimensions, where:

$$q_t(x^d | x^{\setminus d}) = \begin{cases} 1 - \alpha_t & x^d = \text{MASK} \\ \alpha_t q_{0|t}(x^d | x^{\setminus d}) & x^d \neq \text{MASK} \end{cases}, \quad (8)$$

and  $q_{0|t}(x^d | x^{\setminus d})$  is the denoising conditional distribution.

We select the indices to update in the next  $k$  steps  $d_1, \dots, d_k$  by sampling without replacement from the distribution  $\text{Cat}(\frac{\exp(-c_d/\tau)}{\sum_{d'} \exp(-c_{d'}/\tau)})$ , where  $\tau$  is a temperature parameter. This sample can be generated using the Gumbel-top- $k$  trick (Maddison et al., 2014; Kool et al., 2019): First draw  $D$  independent Gumbel random variates,  $g_d \sim \text{Gumbel}(0, 1)$ , one for each dimension. Then rank the dimensions in descending order of  $-c_d/\tau + g_d$  and select the top  $k$  dimensions.

**Parallel updates.** Rather than updating the  $k$  dimensions sequentially, we update them in parallel, as in Hogwild Gibbs sampling (Johnson et al., 2013). We also anneal this temperature so that as  $t \rightarrow 0$  in the sampling procedure, the updates become less random. In doing so, we correct errors in the generation process while minimizing the risk of over-correction harming sample diversity.

**Conditioning on the mask configuration.** In masked diffusion, a sample  $x_t \sim q_t(\cdot)$  contains both mask and non-mask tokens. The Gibbs-inspired update above might turn a mask into a non-mask token or vice versa, and either transition could be undesirable. On the one hand, the corrector steps are not introduced to generate new tokens but rather to fix errors introduced by the predictor steps. On the other, re-masking tokens that the predictor will later unmask creates redundancy. To improve the efficiency of the corrector, instead of the marginal distribution  $q_t(\cdot)$ , we target the mask-conditional distribution,

$$q_t(\cdot | \mathcal{M}(x)) \propto q_t(\cdot) \mathbb{1}_{\mathcal{M}(\cdot) = \mathcal{M}(x)}. \quad (9)$$

In other words, starting from the current sample  $x$ , we fix the mask configuration  $\mathcal{M}(x)$  and only allow the corrector to change non-mask tokens into other non-mask tokens. To update position  $d \in \mathcal{M}(x)$ , we now need to instead sample from the denoising conditional distribution:

$$x^d \sim q_{0|t}(\cdot^d | x^{\setminus d}). \quad (10)$$

Intuitively, this is true because a non-mask token at time  $t$  must be consistent with the token from the true token at time 0 given the masking forward process. This is convenient for us, since the only distribution required by the informed corrector scheme is  $q_{0|t}(x^d | x^{\setminus d})$ . For derivation and more implementation details, see Appendix B.

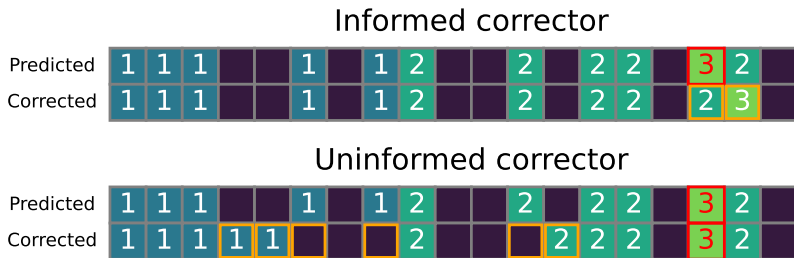


Figure 1: Demonstration of the failure modes of the uninformed corrector on the Markov chain example. The predictor made a mistake (red) in sampling an impossible transition, which is immediately corrected by the informed corrector. The uninformed corrector, however, masks out tokens at random, while unmasking other tokens at the same time. Changes made by the correctors are highlighted in orange.

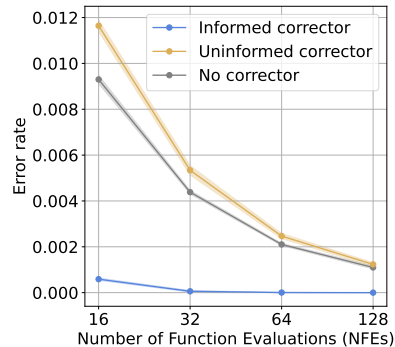


Figure 2: The informed corrector substantially lowers error rates on the Markov chain synthetic experiment.

**Relationship with the (concrete) score function.** The concrete score (Meng et al., 2022; Lou et al., 2023) is an important concept in discrete diffusion that is analogous to the score function in continuous space. The continuous score function is the direction of steepest ascent of the log-likelihood under  $q_t$ , and the concrete score serves a similar purpose, but on a discrete graph topology instead of Euclidean space. Examining the confidence score introduced previously and assuming  $x^d \neq \text{MASK}$ , we see that:

$$q_t(x^d | x^{\setminus d}) = \frac{1 - \alpha_t}{\alpha_t} \frac{q_t(x)}{q_t(M^d(x))} = \frac{1 - \alpha_t}{\alpha_t} s_t(x)_{M^d(x)}^{-1}. \quad (11)$$

See Appendix A.2 for a full derivation. In other words, our confidence score is proportional to the inverse of the concrete score between the states  $x$  and  $M^d(x)$ . Picking the positions with the lowest confidence score is equivalent to picking the positions that would increase the likelihood the most if they were masked out. Therefore, it is intuitive that these positions should be changed by the corrector.

Next, we will discuss how to implement this corrector scheme efficiently, so that only one network evaluation is needed to select and update positions  $d_1, \dots, d_k$  simultaneously.

### 3.2. Parameterizing the Conditional Distribution Using Hollow Transformers

In the last section we established the importance of the denoising conditional distribution  $q_{0|t}(\cdot^d | x^{\setminus d})$ . If we can parameterize and learn this distribution effectively, we can apply the informed corrector scheme. However, the structure of this conditional distribution makes this task challenging: If we want to simultaneously parameterize  $q_{0|t}(\cdot^d | x^{\setminus d})$  for all  $d$  via a neural network, we need to make sure information about  $x^d$  does not propagate to the output at the  $d$ th position.

We solve this problem with a hollow transformer (Sun et al., 2022), a two-stream self-attention architecture where each stream runs causal attention in a different direction. The embeddings are then offset by one position so that the embedding at position  $d$  does not attend to the corresponding input position. The two streams are then summed together and sent through multilayer perceptron layers to the output.

By construction, the hollow transformer satisfies the property that for all  $(t, \theta)$ ,

$$x^{\setminus d} = y^{\setminus d} \implies f^\theta(x, t)_d = f^\theta(y, t)_d, \quad (12)$$

where  $f^\theta(x, t)_d$  represent the output of the network  $f$  at sequence position  $d$  with inputs  $(x, t)$  and parameter  $\theta$ . In other words, the network output at dimension  $d$  is agnostic to the input at the same dimension  $d$ .

To further expand the representation capabilities of the hollow transformer, we propose some changes to the architecture. To better integrate information from different parts of the sequence, we add a separable mixed attention stream that can attend to both the forward and backward causal streams but is forbidden from attending to itself. Instead of combining the two causal streams via summation, we use the final layer of the mixed stream to compute the final outputs of the model. We expand upon architectural details in Appendix C.

### 3.3. Learning the Hollow Transformer with the ELBO

Since the MASK token provides no information about the original data, we make the further observation that

$$q_{0|t}(x^d | x^{\setminus d}) = q_{0|t}(x^d | M^d(x)), \quad (13)$$

which is the familiar denoising distribution that we can approximate using  $p_{0|t}^\theta(x^d | M^d(x)) \approx q_{0|t}(x^d | M^d(x))$ , implemented by the hollow transformer.

The above observation connects us back to the diffusion formalism, as we show in the following simplified diffusion objective derived from (2):

**Proposition 3.1.** *When  $R_t = R_t^{absorb}$ , the continuous-time objective function (2) can be simplified to,*

$$\mathcal{L}_{\overline{\mathcal{M}}}(\theta, x_0) = \int_0^T \mathbb{E}_{q_{t|0}(x|x_0)} \left[ \frac{\alpha'_t}{\alpha_t} \sum_{d \in \overline{\mathcal{M}}(x)} \log p_{0|t}^\theta(x_0^d | M^d(x)) \right] dt + C. \quad (14)$$

This simplification shows that the discrete diffusion loss naturally parameterizes the ELBO in terms of  $p_{0|t}^\theta(x^d | M^d(x))$ . We include a full derivation of this result in Appendix A and show that it is related to  $\mathcal{L}_{\mathcal{M}}$  via a simple label-switching trick. Notably, Campbell et al. (2022) and Shi et al. (2024) both avoid writing the loss in this form, since evaluating  $p_{0|t}^\theta(x^d | M^d(x))$  for each different  $d$  requires a separate call to the denoising network, which is prohibitively inefficient in practice. The hollow transformer fixes this issue, as now the inner sum over  $d$  can be evaluated with one forward pass of the network, making sample estimation of the objective tractable.

Furthermore, we observe that the simplified objective complements the MD4 loss in (5), in the sense that our simplification sums over the non-mask dimensions  $\overline{\mathcal{M}}(x)$ , while MD4 sums over the masked dimensions  $\mathcal{M}(x)$  instead. Both losses ignore half of the learning signal from the sample  $x \sim q_{t|0}(\cdot | x_0)$ , which seems far from ideal. This observation suggests that a more informative objective can be obtained by averaging the two losses:

$$\mathcal{L}_{\text{HD}} = \frac{1}{2}(\mathcal{L}_{\overline{\mathcal{M}}} + \mathcal{L}_{\mathcal{M}}). \quad (15)$$

Since both terms are different versions of the same ELBO objective, our objective can be viewed as applying a variance reduction trick for the sample estimator. In Appendix E we observe that this objective indeed outperforms its individual components and makes training converge faster.

## 4. Related Work

**Iterative generation of discrete data.** Parallel to the line of work on discrete diffusion models, other classes of discrete models that implement similar ideas of iterative generation have been developed. This includes SUN-DAE (Savinov et al., 2021), SDDM (Sun et al., 2022), and MaskGIT (Chang et al., 2022). These models typically do not formally define a forward and backward process and are trained by an objective that does not necessarily correspond to maximizing the likelihood of data, such as a non-likelihood-weighted denoising loss (Chang et al., 2022) or a generalization of ratio-matching losses (Sun et al., 2022).

Despite the heuristic loss, the MaskGIT model, combined with a vector-quantized (VQ) autoencoder, produces high quality ImageNet samples in 8-16 steps. In contrast, discrete diffusion models equipped with or without VQ latents (Gu et al., 2022; Shi et al., 2024) still requires hundreds of steps to produce a high-quality ImageNet sample. Our work represents a significant step towards closing this gap.

**Predictor-corrector sampling.** Song et al. (2021) introduced predictor-corrector samplers for continuous diffusion models, and Campbell et al. (2022) introduced the forward-backward correctors for discrete diffusion. However, this “uninformed” corrector can only address errors through random re-masking, due to the transition rate being a sum of forward and backward rates. Relatedly, Lezama et al. (2022) proposed a corrector scheme to improve MaskGIT sampling. Compared to our method, they learn an additional corrector kernel besides the main model and require more steps to achieve good sample quality.

## 5. Experiments

We now turn to an empirical evaluation of informed correctors. In Section 5.1, we test the informed corrector against other sampling methods in a hidden Markov model setting where the true denoising conditional distribution is known. We find that informed correctors consistently reduce error rates across a wide range of function evaluation counts. In Section 5.2, we use informed correctors for tokenized image synthesis using the tokenization model of Chang et al. (2022). Our method demonstrates strong performance on ImageNet  $256 \times 256$ , achieving competitive FID scores with a 230M parameter model and only a small number of function evaluations.

### 5.1. Hidden Markov Modeling

To check if informed correctors improve sample quality, we propose a simple setting where the true denoising conditional distribution  $q_t$  is easily accessible. Consider sequence data  $x \in \{0, \dots, S-1\}^D$  sampled from a Markov chain:

$$q_0(x) = q_0(x^1) \prod_{d=2}^D q_0(x^d | x^{d-1}), \quad (16)$$

where  $q_0(x^d = i | x^{d-1} = j) = A_{ij}$  and  $x^1$  is sampled uniformly. At time  $t$  of the forward process, the denoising model observes a masked version of this sequence:

$$q_{t|0}(x_t | x_0) = \prod_{d=1}^D q_{t|0}(x_t^d | x_0^d) \quad (17)$$

$$= \prod_{d=1}^D \left\{ \alpha_t \mathbb{1}_{\{x_t^d = x_0^d\}} + (1 - \alpha_t) \mathbb{1}_{\{x_t^d = \text{MASK}\}} \right\}, \quad (18)$$

and tries to predict the conditional denoising likelihood  $q_{0|t}(x_0^d | x_t^{\setminus d})$ . This can be seen as performing inference in a hidden Markov model (HMM), where the prior is the Markov chain  $q_0$ , and the observation model is  $q_{t|0}$ . Given this, we can perform standard message-passing inference (Murphy, 2012) to find the posterior  $q_{0|t}(x_0^d | x_t^{\setminus d})$ .

To demonstrate the problems with existing samplers, we choose a structured transition matrix  $A$ :

$$A_{ij} = \begin{cases} p & j = i \\ 1 - p & j = (i + 1) \bmod S \\ 0 & \text{otherwise.} \end{cases} \quad (19)$$

At each position, the token  $x^d$  has probability  $p$  of staying fixed and probability  $1 - p$  of changing into the next token. To evaluate sample quality, one important metric is the number of errors in the samples, i.e., occurrences of impossible transitions within the sampled sequence. The overall error rate is computed by:

$$r_{\text{err}}((\hat{x}_n)_{n=1}^N) = \frac{1}{N(D-1)} \sum_{n=1}^N \sum_{d=1}^{D-1} \mathbb{1}_{\{\hat{x}_n^{d+1} \neq \hat{x}_n^d\}} \cdot \mathbb{1}_{\{\hat{x}_n^{d+1} \neq (\hat{x}_n^d - 1) \bmod S\}}. \quad (20)$$

Since the samplers have access to the true denoising distribution, the error rate will be 0 if no more than one token is generated in a single step. However, if more than one token is generated during a parallel update, there is a risk of generating impossible transitions.

In this illustrative experiment we use vocabulary size  $S = 4$  and sequence length  $D = 128$  and set the “stickiness”  $p$  to 0.9. The masking schedule  $\alpha_t$  is set to a cosine schedule as in Shi et al. (2024). Hyperparameters for informed correctors are tuned for each different number of function evaluations (NFE) setting (see Appendix D). For samplers with correctors, we take one corrector step after each predictor step. The NFE is then equal to the sum of the total number of predictor steps and corrector steps.

We show the mean and standard deviation of error rates achieved by different sampling strategies over 5 random seeds in Figure 2. We find that ancestral sampling with the informed corrector yields the least error for all examined NFE settings. Meanwhile, the uninformed corrector consistently performs worse than using no corrector at all. This shows that an uninformed corrector step is not as valuable as an additional predictor step in this setting. We demonstrate why the uninformed corrector fails in a pictorial example in Figure 1.

## 5.2. Class-conditional Image Modeling

We now evaluate the performance of our method on tokenized ImageNet-256. The training set is cropped to  $256 \times 256$  pixels and divided into 256 patches of size  $16 \times 16$ . A pretrained VQ-VAE tokenizer (Gu et al., 2022) is then used to encode the patches into  $S = 1024$  different discrete tokens. For the architecture details of the hollow transformer, see Appendix C. The denoising model is trained with our HollowDiff objective (15) for 2.5M iterations. We use the predictor-corrector sampling scheme with informed corrector to generate from the learned model. We report four standard quality metrics, Fréchet inception distance (FID), Inception score (IS), precision, and recall (Kynkäänniemi et al., 2019), and compare performance with twelve state-of-the-art generative models in Table 1. We see that the HollowDiff demonstrates competitive performance among diffusion models. Specifically, it substantially outperforms the previous best discrete diffusion result by VQ-Diffusion (6.45 FID vs. 11.89) using a smaller model and many fewer sampling steps (17 vs. 100). Figure 3 displays example informed corrector generations.



Figure 3: Example robin images generated from our ImageNet  $256 \times 256$  model using informed correctors.

**Comparison with different samplers.** We compare the FID values obtained with different samplers under a range of NFEs to demonstrate how the informed corrector improves sample quality. We follow the same setting as in Section 5.1, applying one corrector step after each predictor step. We found empirically that applying a final update of the form

$$\hat{x}_0^d = \operatorname{argmax}_{x_0^d} p_{0|t}^\theta(x_0^d | \hat{x}_t^{\setminus d}) \quad (21)$$

for all  $d \in \{1, \dots, D\}$  significantly improves the results. Our intuition is that this final update helps eliminate remaining noise and local errors from all positions. To keep the

Table 1: A comparison of state-of-the-art generative model results on ImageNet  $256 \times 256$ . For our method we show results with 8 predictor steps, 8 corrector steps, and 1 argmax step. Among diffusion models, HollowDiff with informed corrector yields competitive performance with fewer evaluation steps and lower parameter count.

Model type	Method	# Params	# Steps	FID ↓	IS ↑	Precision ↑	Recall ↑
Non-diffusion	VQVAE-2 (Razavi et al., 2019)	13.5B	5120	31.11	45	0.36	0.57
	VQGAN (Esser et al., 2021)	1.3B	256	15.78	78.3	-	-
	RQ-Transformer (Lee et al., 2022)	3.8B	256	7.55	137	-	-
	VIT-VQ+VIM (Yu et al., 2021)	1.7B	1024	4.17	175.1	-	-
	MaskGIT (Chang et al., 2022)	227M	8	6.18	182.1	<b>0.80</b>	0.51
	DPC (Lezama et al., 2022)	391M	180	4.45	<b>244.8</b>	0.78	0.52
	StraIT (Qian et al., 2023)	863M	12	<b>3.96</b>	214.1	0.74	<b>0.62</b>
Cont. diffusion (pixel)	Improved DDPM (Nichol & Dhariwal, 2021)	280M	250	12.26	-	<b>0.70</b>	0.62
	CDM (Ho et al., 2022)	~1B	250	<b>4.88</b>	<b>158.71</b>	-	-
	ADM (Dhariwal & Nichol, 2021)	554M	250	10.94	101.0	0.69	<b>0.63</b>
Cont. diffusion (latent)	LDM (Rombach et al., 2022)	400M	250	<b>10.56</b>	<b>103.49</b>	<b>0.71</b>	<b>0.62</b>
Discrete diffusion	VQ-Diffusion (Gu et al., 2022)	518M	100	11.89	-	-	-
	Informed corrector (Ours)	230M	17	<b>6.45</b>	<b>185.91</b>	<b>0.78</b>	0.45
	Ablation:						
	- No corrector	230M	17	10.24	123.87	0.71	<b>0.52</b>
- Uninformed corrector	230M	17	10.93	123.64	0.70	0.51	

comparison fair, we use this argmax update for all samplers by default. We search hyperparameters for each NFE setting individually and plot the lowest FID in Figure 4. We see that the uncorrected ancestral sampling baseline yields the overall worst performance, followed by the uninformed corrector, which greatly improves sample quality as NFEs increase. Interestingly, the uninformed corrector is worse than the baseline at the lowest NFEs, suggesting that in this regime applying the uninformed corrector is less valuable than simply having extra predictor steps. By contrast, MaskGIT performs very well in the low NFE regimes, but quickly saturates and becomes tricky to tune when the number of steps increases.

Our informed corrector consistently yields the best performance across NFEs, with substantial improvements in both the low NFE and high NFE regimes over the uncorrected ancestral sampling baseline. In summary, we find that informed correctors materially improve sample quality in discrete-latent diffusion models, enabling fast, high-quality image generation in just a few steps.

## 6. Discussion

We proposed informed correctors and a training framework for learning and sampling from masked discrete diffusion models. We showed that the usual uninformed forward-backward corrector is not well-suited to the masked diffusion setting, since it does not leverage information about the conditional likelihood of the generated tokens. To address this problem, we introduce a novel solution combining an informed corrector, a hollow transformer architecture, and

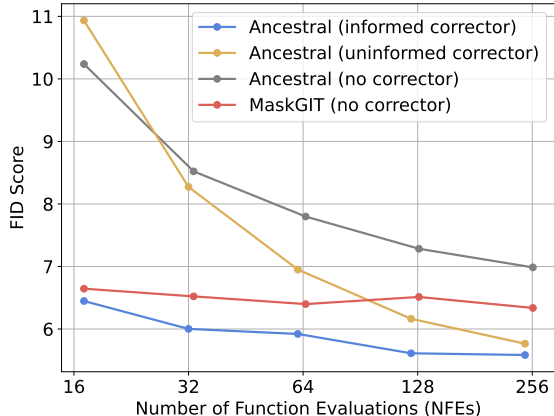


Figure 4: FID comparison between different samplers on our trained model. Ancestral sampling with informed corrector outperforms alternative methods across different NFEs.

an improved training strategy (HollowDiff) that maximizes learning signals per iteration. Our approach produces superior sample quality with fewer model evaluations than alternative discrete diffusion samplers both in the synthetic setting and on ImageNet  $256 \times 256$ . Overall, our work serves to further enhance the capabilities of diffusion models in discrete regimes and to bridge the sampling efficiency gap between discrete diffusion models and other types of generative models.

**Limitations and future work.** Using the informed correctors for absorbing diffusion requires the use of the hollow transformer architecture. As a result, we cannot apply the correctors directly to arbitrary pretrained models. The large scale results presented in this work are also limited to the

image domain, and we would like to see the informed corrector work on other challenging generative modeling tasks such as predicting protein sequences or language modeling.

In developing the informed corrector, we observed that design decisions in the training and sampling phases can be strongly coupled. Future work could explore this coupling in more depth, for example, by studying how the architecture and training objective can be further adapted to enable efficient sampling strategies.

## Acknowledgements

This research was supported with Cloud TPUs from Google’s TPU Research Cloud (TRC). Y.Z. was partially supported by the Stanford Interdisciplinary Graduate Fellowship (SIGF). S.D. and F.C. were partially supported by the McKnight Foundation, the Simons Foundation and an NIH CRCNS grant R01DC020874. S.W.L. was supported in part by fellowships from the Simons Collaboration on the Global Brain, the Alfred P. Sloan Foundation, and the McKnight Foundation. In addition, we would like to thank Matthew Mackay for his notes on continuous time discrete diffusion and Jimmy Smith and Xavier Gonzalez for their help and feedback throughout this project.

## Impact Statement

This paper presents work whose goal is to advance the field of Machine Learning. There are many potential societal consequences of our work, none which we feel must be specifically highlighted here.

## References

- Alamdari, S., Thakkar, N., van den Berg, R., Lu, A., Fusi, N., Amini, A., and Yang, K. Protein generation with evolutionary diffusion: sequence is all you need. In *NeurIPS Generative AI and Biology (GenBio) Workshop*, 2023.
- Austin, J., Johnson, D. D., Ho, J., Tarlow, D., and Van Den Berg, R. Structured denoising diffusion models in discrete state-spaces. *Advances in Neural Information Processing Systems*, 34:17981–17993, 2021.
- Benton, J., Shi, Y., De Bortoli, V., Deligiannidis, G., and Doucet, A. From denoising diffusions to denoising Markov models. *Journal of the Royal Statistical Society Series B: Statistical Methodology*, 86(2):286–301, 2024.
- Campbell, A., Benton, J., De Bortoli, V., Rainforth, T., Deligiannidis, G., and Doucet, A. A continuous time framework for discrete denoising models. *Advances in Neural Information Processing Systems*, 35:28266–28279, 2022.
- Chang, H., Zhang, H., Jiang, L., Liu, C., and Freeman, W. T. MaskGIT: Masked generative image transformer. In *Proceedings of the IEEE/CVF Conference on Computer Vision and Pattern Recognition*, pp. 11315–11325, 2022.
- Devlin, J., Chang, M.-W., Lee, K., and Toutanova, K. BERT: Pre-training of deep bidirectional transformers for language understanding. *arXiv preprint arXiv:1810.04805*, 2018.
- Dhariwal, P. and Nichol, A. Diffusion models beat GANs on image synthesis. *Advances in Neural Information Processing Systems*, 34:8780–8794, 2021.
- Esser, P., Rombach, R., and Ommer, B. Taming transformers for high-resolution image synthesis. In *Proceedings of the IEEE/CVF Conference on Computer Vision and Pattern Recognition*, pp. 12873–12883, 2021.
- Gu, S., Chen, D., Bao, J., Wen, F., Zhang, B., Chen, D., Yuan, L., and Guo, B. Vector quantized diffusion model for text-to-image synthesis. In *Proceedings of the IEEE/CVF Conference on Computer Vision and Pattern Recognition*, pp. 10696–10706, 2022.
- Ho, J., Jain, A., and Abbeel, P. Denoising diffusion probabilistic models. *Advances in Neural Information Processing Systems*, 33:6840–6851, 2020.
- Ho, J., Saharia, C., Chan, W., Fleet, D. J., Norouzi, M., and Salimans, T. Cascaded diffusion models for high fidelity image generation. *Journal of Machine Learning Research*, 23(47):1–33, 2022.
- Hoogeboom, E., Gritsenko, A. A., Bastings, J., Poole, B., Berg, R. v. d., and Salimans, T. Autoregressive diffusion models. *arXiv preprint arXiv:2110.02037*, 2021a.
- Hoogeboom, E., Nielsen, D., Jaini, P., Forré, P., and Welling, M. Argmax flows and multinomial diffusion: Learning categorical distributions. *Advances in Neural Information Processing Systems*, 34:12454–12465, 2021b.
- Johnson, M. J., Saunderson, J., and Willsky, A. Analyzing Hogwild parallel Gaussian Gibbs sampling. *Advances in Neural Information Processing Systems*, 26, 2013.
- Kool, W., Van Hoof, H., and Welling, M. Stochastic beams and where to find them: The Gumbel-top-k trick for sampling sequences without replacement. In *International Conference on Machine Learning*, pp. 3499–3508. PMLR, 2019.
- Kynkäänniemi, T., Karras, T., Laine, S., Lehtinen, J., and Aila, T. Improved precision and recall metric for assessing generative models. *Advances in Neural Information Processing Systems*, 32, 2019.

- Latuszyński, K., Roberts, G. O., and Rosenthal, J. S. Adaptive Gibbs samplers and related MCMC methods. *The Annals of Applied Probability*, pp. 66–98, 2013.
- Lee, D., Kim, C., Kim, S., Cho, M., and Han, W.-S. Autoregressive image generation using residual quantization. In *Proceedings of the IEEE/CVF Conference on Computer Vision and Pattern Recognition*, pp. 11523–11532, 2022.
- Levine, R. A. and Casella, G. Optimizing random scan Gibbs samplers. *Journal of Multivariate Analysis*, 97(10): 2071–2100, 2006.
- Levine, R. A., Yu, Z., Hanley, W. G., and Nitao, J. J. Implementing random scan Gibbs samplers. *Computational Statistics*, 20(1):177–196, 2005.
- Lezama, J., Salimans, T., Jiang, L., Chang, H., Ho, J., and Essa, I. Discrete predictor-corrector diffusion models for image synthesis. In *International Conference on Learning Representations*, 2022.
- Loshchilov, I. and Hutter, F. Decoupled weight decay regularization, 2019.
- Lou, A., Meng, C., and Ermon, S. Discrete diffusion language modeling by estimating the ratios of the data distribution. *arXiv preprint arXiv:2310.16834*, 2023.
- Maddison, C. J., Tarlow, D., and Minka, T. A\* sampling. *Advances in Neural Information Processing Systems*, 27, 2014.
- Mahoney, M. Text8 dataset. <http://mattmahoney.net/dc/textdata.html>, 2006.
- Meng, C., Choi, K., Song, J., and Ermon, S. Concrete score matching: Generalized score matching for discrete data. *Advances in Neural Information Processing Systems*, 35: 34532–34545, 2022.
- Mitliagkas, I. and Mackey, L. Improving Gibbs sampler scan quality with DoGS. In *International Conference on Machine Learning*, pp. 2469–2477. PMLR, 2017.
- Murphy, K. P. *Machine Learning: A Probabilistic Perspective*. MIT Press, 2012.
- Nichol, A. Q. and Dhariwal, P. Improved denoising diffusion probabilistic models. In *International Conference on Machine Learning*, pp. 8162–8171. PMLR, 2021.
- Ou, J., Nie, S., Xue, K., Zhu, F., Sun, J., Li, Z., and Li, C. Your absorbing discrete diffusion secretly models the conditional distributions of clean data. *arXiv preprint arXiv:2406.03736*, 2024.
- Qian, S., Chang, H., Li, Y., Zhang, Z., Jia, J., and Zhang, H. StraIT: Non-autoregressive generation with stratified image transformer. *arXiv preprint arXiv:2303.00750*, 2023.
- Ramesh, A., Pavlov, M., Goh, G., Gray, S., Voss, C., Radford, A., Chen, M., and Sutskever, I. Zero-shot text-to-image generation. In *International Conference on Machine Learning*, pp. 8821–8831. Pmlr, 2021.
- Razavi, A., Van den Oord, A., and Vinyals, O. Generating diverse high-fidelity images with VQ-VAE-2. *Advances in Neural Information Processing Systems*, 32, 2019.
- Rombach, R., Blattmann, A., Lorenz, D., Esser, P., and Ommer, B. High-resolution image synthesis with latent diffusion models. In *Proceedings of the IEEE/CVF Conference on Computer Vision and Pattern Recognition*, pp. 10684–10695, 2022.
- Sahoo, S. S., Arriola, M., Schiff, Y., Gokaslan, A., Marroquin, E., Chiu, J. T., Rush, A., and Kuleshov, V. Simple and effective masked diffusion language models. *arXiv preprint arXiv:2406.07524*, 2024.
- Santos, J. E., Fox, Z. R., Lubbers, N., and Lin, Y. T. Black-out diffusion: Generative diffusion models in discrete-state spaces. *arXiv preprint arXiv:2305.11089*, 2023.
- Savinov, N., Chung, J., Binkowski, M., Elsen, E., and van den Oord, A. Step-unrolled denoising autoencoders for text generation. In *International Conference on Learning Representations*, 2021.
- Shi, J., Han, K., Wang, Z., Doucet, A., and Titsias, M. K. Simplified and generalized masked diffusion for discrete data. *arXiv preprint arXiv:2406.04329*, 2024.
- Sohl-Dickstein, J., Weiss, E., Maheswaranathan, N., and Ganguli, S. Deep unsupervised learning using nonequilibrium thermodynamics. In *International Conference on Machine Learning*, pp. 2256–2265. PMLR, 2015.
- Song, J., Meng, C., and Ermon, S. Denoising diffusion implicit models. In *International Conference on Learning Representations*, 2020.
- Song, Y. and Ermon, S. Generative modeling by estimating gradients of the data distribution. *Advances in Neural Information Processing Systems*, 32, 2019.
- Song, Y., Sohl-Dickstein, J., Kingma, D. P., Kumar, A., Ermon, S., and Poole, B. Score-based generative modeling through stochastic differential equations. In *International Conference on Learning Representations*, 2021.
- Sun, H., Yu, L., Dai, B., Schuurmans, D., and Dai, H. Score-based continuous-time discrete diffusion models. *arXiv preprint arXiv:2211.16750*, 2022.

- Vignac, C., Krawczuk, I., Siraudin, A., Wang, B., Cevher, V., and Frossard, P. DiGress: Discrete denoising diffusion for graph generation. In *The Eleventh International Conference on Learning Representations*, 2023.
- Watson, J. L., Juergens, D., Bennett, N. R., Trippe, B. L., Yim, J., Eisenach, H. E., Ahern, W., Borst, A. J., Ragotte, R. J., Milles, L. F., et al. De novo design of protein structure and function with RFdiffusion. *Nature*, 620 (7976):1089–1100, 2023.
- Yang, Z. XLNet: Generalized autoregressive pre-training for language understanding. *arXiv preprint arXiv:1906.08237*, 2019.
- Yu, J., Li, X., Koh, J. Y., Zhang, H., Pang, R., Qin, J., Ku, A., Xu, Y., Baldrige, J., and Wu, Y. Vector-quantized image modeling with improved VQGAN. *arXiv preprint arXiv:2110.04627*, 2021.
- Zanella, G. Informed proposals for local MCMC in discrete spaces. *Journal of the American Statistical Association*, 2019.
- Zheng, L., Yuan, J., Yu, L., and Kong, L. A reparameterized discrete diffusion model for text generation. *arXiv preprint arXiv:2302.05737*, 2023.

## A. Diffusion Objectives

### A.1. Unifying diffusion and score entropy

In this section we derive the simplified objective in Shi et al. (2024); Sahoo et al. (2024); Ou et al. (2024). We start from Campbell et al. (2022)'s continuous time discrete diffusion ELBO objective. For clarity, we use variable names  $x$ ,  $y$ , and  $z$  in a way that indicates temporal order:

$$\mathcal{L}(\theta) = \int \mathbb{E}_{q_t(y)r_t(z|y)} \left[ \left\{ \sum_{x' \neq y} \tilde{R}_t^\theta(y, x') \right\} - \left\{ \sum_{z' \neq y} R_t(y, z') \right\} \log(\tilde{R}_t^\theta(z, y)) \right] dt \quad (22)$$

$$= \int \mathbb{E}_{q_t(y)r_t(z|y)} \left[ \tilde{R}_t^\theta(y) - R_t(y) \log(\tilde{R}_t^\theta(z, y)) \right] dt, \quad (23)$$

where  $R_t(y) \triangleq -R_t(y, y) = \sum_{z' \neq y} R_t(y, z')$ . Here  $r_t$  represents the probability of a specific transition, given that a transition happens at time  $t$ :

$$r_t(z | y) = \begin{cases} \frac{R_t(y, z)}{R_t(y)} & y \neq z \\ 0 & y = z. \end{cases} \quad (24)$$

Campbell et al. (2022) rewrote the joint distribution

$$q_t(y)r_t(z | y) = \sum_{x_0} q_0(x_0)\psi_t(z | x_0)\phi_t(y | z, x_0) \quad (25)$$

and then analytically integrated out  $y$  to reduce sampling variance, given factorization assumptions on  $R_t$ . The downside of this approach is that the resulting loss becomes very complicated and unintuitive.

To circumvent this complication, we propose to instead rewrite the objective with a label switching trick:

$$\mathcal{L}(\theta) = \int \mathbb{E}_{q_0(x_0)q_t(y|x_0)r_t(z|y)} \left[ \tilde{R}_t^\theta(y) - R_t(y) \log(\tilde{R}_t^\theta(z, y)) \right] dt \quad (26)$$

$$= \int \mathbb{E}_{q_0(x_0)q_t(y|x_0)} \left[ \tilde{R}_t^\theta(y) - \sum_{z \neq y} R_t(y, z) \log(\tilde{R}_t^\theta(z, y)) \right] dt \quad (27)$$

$$= \int \mathbb{E}_{q_0(x_0)q_t(y|x_0)} \left[ \sum_{z \neq y} \tilde{R}_t^\theta(y, z) - \sum_{z \neq y} R_t(y, z) \log(\tilde{R}_t^\theta(z, y)) \right] dt \quad (28)$$

$$= \int \mathbb{E}_{q_0(x_0)} \left[ \sum_y \sum_{z \neq y} \left\{ q_t(y | x_0) \tilde{R}_t^\theta(y, z) - q_t(y | x_0) R_t(y, z) \log(\tilde{R}_t^\theta(z, y)) \right\} \right] dt \quad (29)$$

$$= \int \mathbb{E}_{q_0(x_0)} \left[ \sum_y \sum_{z \neq y} \left\{ q_t(y | x_0) \tilde{R}_t^\theta(y, z) - q_t(z | x_0) R_t(z, y) \log(\tilde{R}_t^\theta(y, z)) \right\} \right] dt. \quad (30)$$

Note that we switched the labels  $y$  and  $z$  on the last line, which is the key trick that simplified our derivation. Proceeding from line (30) becomes straightforward:

$$\mathcal{L}(\theta) = \int \mathbb{E}_{q_0(x_0)q_t(y|x_0)} \left[ \sum_{z \neq y} \left\{ \tilde{R}_t^\theta(y, z) - R_t(z, y) \frac{q_t(z | x_0)}{q_t(y | x_0)} \log(\tilde{R}_t^\theta(y, z)) \right\} \right] dt \quad (31)$$

$$= \int \mathbb{E}_{q_0(x_0)q_t(y|x_0)} \left[ \sum_{x \neq y} \left\{ \tilde{R}_t^\theta(y, x) - \tilde{R}_t^\theta(y, x) \log(\tilde{R}_t^\theta(y, x)) \right\} \right] dt, \quad (32)$$

where  $\tilde{R}_{t|0}(y, x) \equiv R_t(x, y) \frac{q_t(x|x_0)}{q_t(y|x_0)}$  is the true reverse transition rate conditioned on  $x_0$ , and we renamed  $z$  to  $x$  to preserve alphabetical order of the variables for readability. Now we have a simple Monte Carlo estimator for this objective: we just need to sample  $y$  from the marginal distribution and then evaluate the parameterized transition model  $\tilde{R}_t^\theta(y, x)$  for all neighbors  $x$  of  $y$ , which can be done using only one model evaluation.

Note again that we can use the score parameterization for the reverse process:

$$\tilde{R}_t^\theta(z, y) = R_t(y, z) s_t^\theta(z, y). \quad (33)$$

Plugging this parameterization into (32) and absorbing constant terms into  $C$ , we get the diffusion weighted denoising score entropy objective (Theorem 3.6 of Lou et al. (2023)):

$$\mathcal{L}_{DSE} = \int \mathbb{E}_{q_0(x_0)q_t(y|x_0)} \left[ R_t(x, y) \sum_{x \neq y} \left\{ s_t^\theta(y, x) - \frac{q_t(x|x_0)}{q_t(y|x_0)} \log(s_t^\theta(y, x)) \right\} \right] + C dt. \quad (34)$$

## A.2. Simplifying the Score Function for Masked Diffusion

The relationship between the (concrete) score function and denoising distribution can be simplified in the case of masked diffusion. We first start with the relation between the denoising distribution and score function in (Campbell et al., 2022):

$$s_t(y)_x = \frac{q_t(x)}{q_t(y)} = \sum_{x_0} \frac{q_{t|0}(x|x_0)}{q_{t|0}(y|x_0)} q_{0|t}(x_0|y). \quad (35)$$

For a state  $x$  where  $x^d \neq \text{MASK}$ , consider the score from  $M^d(x)$  to  $x$ :

$$s_t^\theta(M^d(x))_x = \sum_{x_0} \frac{q_{t|0}(x|x_0)}{q_{t|0}(M^d(x)|x_0)} p_{0|t}^\theta(x_0|M^d(x)) \quad (36)$$

$$= \sum_{x_0^d} \frac{q_{t|0}(x^d|x_0^d)}{q_{t|0}(\text{MASK}|x_0^d)} p_{0|t}^\theta(x_0^d|M^d(x)) \quad (37)$$

$$= \frac{q_{t|0}(x^d|x^d)}{q_{t|0}(\text{MASK}|x^d)} p_{0|t}^\theta(x^d|M^d(x)) \quad (38)$$

$$= \frac{\alpha_t}{1 - \alpha_t} p_{0|t}^\theta(x^d|M^d(x)) \quad (39)$$

where  $\alpha_t$  represents the survival probability of any non-mask token at time  $t$ , which is assumed to be constant for all dimensions and token values. Going from (37) to (38) we used the fact that  $x^d = x_0^d$  if  $x^d \neq \text{MASK}$ . This formula tells us that in the case of masking diffusion, the score function between mask and non-mask tokens is just a constant factor away from the denoising distribution.

In this work, we use a hollow transformer  $f^\theta$  that outputs a  $D \times S$  array, and we use  $f^\theta(x, t)_{d,s}$  to represent  $p_{0|t}^\theta(x^d = s | M^d(x))$ . We can also omit the  $t$  dependence of the network here because in absorbing state diffusion the true  $q_{0|t}(x^d | M^d(x))$  does not depend on  $t$  (proof omitted).

## A.3. Deriving the HollowDiff Objective

The hollow transformer provides us with a way to optimize the optimize the TauLDR objective (23) directly:

$$-\log p(x_0) \leq \mathcal{L}(\theta) = \int_0^T \mathbb{E}_{q_{t|0}(y|x_0)r_t(z|y)} \left[ \tilde{R}_t^\theta(y) - R_t(y) \log(\tilde{R}_t^\theta(z, y)) \right] dt + C, \quad (40)$$

$$= \int_0^T \mathbb{E}_{q_{t|0}(y|x_0)} \left[ \sum_{x \neq y} R_t(x, y) s_t^\theta(y)_x - \sum_{z \neq y} R_t(y, z) \log(\tilde{R}_t^\theta(z, y)) \right] dt + C \quad (41)$$

$$= \int_0^T \mathbb{E}_{q_{t|0}(y|x_0)} \left[ \sum_{x \neq y} R_t(x, y) s_t^\theta(y)_x - \sum_{z \neq y} R_t(y, z) \log(s_t^\theta(z)_y) \right] dt + C. \quad (42)$$

Notice that we can further simplify the second term by leveraging the sparsity structure of the forward process:

$$\sum_{z \neq y} R_t(y, z) \log(s_t^\theta(z)_y) = \sum_{d \in \overline{\mathcal{M}}(y)} R_t(y, M^d(y)) \log(s_t^\theta(M^d(y))_y), \quad (43)$$

$$= \sum_{d \in \overline{\mathcal{M}}(y)} R_t(y, M^d(y)) \log\left(\frac{\alpha_t}{1 - \alpha_t} f^\theta(y)_{d, y^d}\right), \quad (44)$$

$$= -\frac{\alpha'_t}{\alpha_t} \sum_{d \in \overline{\mathcal{M}}(y)} \log(f^\theta(y)_{d, y^d}) + C, \quad (45)$$

where  $\alpha'_t$  represent the time derivative of  $\alpha_t$ . Note that here we used the hollow property  $f^\theta(y)_d = f^\theta(M^d(y))_d$ , which allows us to evaluate the sum over  $d \in \overline{\mathcal{M}}(y)$  using only one function evaluation of  $f$ . Similarly we can write out the first term, which conveniently reduces to a constant due to the structure of the forward process:

$$\sum_{x \neq y} R_t(x, y) s^\theta(y)_x = \frac{\alpha_t}{1 - \alpha_t} \sum_{d \in \mathcal{M}(y)} \sum_{\substack{x: x^d \neq \text{MASK}, \\ x \setminus^d = y \setminus^d}} R_t(x, y) f^\theta(y)_{d, x^d} \quad (46)$$

$$= -\frac{\alpha'_t}{1 - \alpha_t} \sum_{d \in \mathcal{M}(y)} \sum_{\substack{x: x^d \neq \text{MASK}, \\ x \setminus^d = y \setminus^d}} f^\theta(y)_{d, x^d} = -\frac{\alpha'_t}{1 - \alpha_t} |\mathcal{M}(y)|. \quad (47)$$

Here we are using the fact that  $f^\theta(y)_d$  is a vector representing the distribution over the non-mask tokens and therefore sums to 1. Putting these back together, we have:

$$\mathcal{L}(\theta) = \int_0^T \frac{\alpha'_t}{\alpha_t} \mathbb{E}_{q_{t|0}(y|x_0)} \left[ \sum_{d \in \overline{\mathcal{M}}(y)} \log(f^\theta(y)_{d, y^d}) \right] dt + C, \quad (48)$$

which is very similar to the MD4 loss (5) of Shi et al. (2024), except that the sum over all mask positions is replaced with the sum over all *non-mask* positions and the coefficients are different.

In practice, we want to maximize learning signals for the model. Since the objective (48) only uses the non-mask dimensions of  $y$ , we propose to combine it with the MD4 objective which uses the mask dimensions instead. These two simplified objectives are mathematically equivalent and have the same optima, but can suggest different stochastic gradient estimates. The combined objective is then

$$\mathcal{L}(\theta) = \int_0^T \frac{1}{2} \mathbb{E}_{q_{t|0}(y|x_0)} \left[ \frac{\alpha'_t}{\alpha_t} \sum_{d \in \overline{\mathcal{M}}(y)} \log(f^\theta(y)_{d, x_0^d}) + \frac{\alpha'_t}{1 - \alpha_t} \sum_{d \in \mathcal{M}(y)} \log(f^\theta(y)_{d, x_0^d}) \right] dt + C, \quad (49)$$

where we have changed the index in the first term from  $y^d$  to  $x_0^d$  for consistency, since  $y^d = x_0^d$  when  $d$  is an unmasked dimension. Note that the HollowDiff objective leads to a lower-variance stochastic gradient estimator, as it leverages more learning signal for a single sample of  $y$ . We confirm this empirically via loss curves in Appendix E.

## B. Informed Corrector

We explore informed corrector updates that leverages the hollow transformer architecture. Specifically, we consider the Gibbs operator:

$$q_t(x^d | x \setminus^d) = \sum_{x_0^d} q_{t|0}(x^d | x_0^d) q_{0|t}(x_0^d | x \setminus^d) = \alpha_t q_{0|t}(x^d | x \setminus^d) \mathbb{1}_{\{x^d \neq \text{MASK}\}} + (1 - \alpha_t) \mathbb{1}_{\{x^d = \text{MASK}\}}. \quad (50)$$

To approximate this operator, we can use the learned network  $f^\theta(x)_{d,i}$  in the place of  $q_{0|t}(x^d = i | x \setminus^d)$ , since the hollow transformer architecture blocks out information of  $x^d$  on the  $d$ th output dimension.

In order to reach the stationary distribution  $q_t(x)$ , we need to repeat the Gibbs update, iterating over all dimensions  $d$ . This is very inefficient in realistic settings. Instead, we choose to prioritize updates on the ‘‘most unlikely’’ dimensions, where  $x^d$

is most likely to be affected by the compounding errors in the simulation of the backward process. To achieve this, we rank the dimensions according to the confidence score  $c_d \triangleq \log q_t(x^d | x^{\setminus d})$  and perform  $k$  updates at the same time.

One observation is that changing the mask configuration does not actually do anything useful for us, since the mask configuration does not contain any information. This suggests that we should instead consider the distribution conditioning on the mask configuration:

$$q_t(x^d | x^{\setminus d}, x^d \neq \text{MASK}) = \sum_{x_0^d} q_{t|0}(x^d | x_0^d, x^d \neq \text{MASK}) q_{0|t}(x_0^d | x^{\setminus d}, x^d \neq \text{MASK}) \quad (51)$$

$$= \sum_{x_0^d} \mathbb{1}_{\{x^d \neq \text{MASK}\}} \mathbb{1}_{\{x^d = x_0^d\}} q_{0|t}(x_0^d | x^{\setminus d}) \quad (52)$$

$$= \mathbb{1}_{\{x^d \neq \text{MASK}\}} q_{0|t}(x^d | x^{\setminus d}). \quad (53)$$

Repeatedly applying this operator on the non-masked dimensions creates a Markov chain with the stationary distribution equal to  $q_t(x | \mathcal{M}_t) \triangleq q_t(x | x^{\mathcal{M}_t} = \text{MASK})$  where  $\mathcal{M}_t$  is the set of masked indices after the predictor update.

This translates to a straightforward procedure: find the non-mask dimensions with the lowest scores, and then sample from the model predictions  $p_{0|t}^\theta(x^d | x^{\setminus d})$  of that dimension. For real-world datasets, we found that doing an argmax update in the end, where all dimensions are updated to the token that maximizes the conditional likelihood can be helpful for sample quality. We also follow [Campbell et al. \(2022\)](#) and apply the corrector only when  $t < t_c$ . We set entry time  $t_c = 0.9$  and number of correctors  $C = 1$  for the majority of our experiments. The algorithm is outlined in [Algorithm 1](#) below.

---

**Algorithm 1** Backward process with informed corrector steps

---

**Require:**  $f, t_{min}, t_c, \theta$ , temperature  $\tau$ ;

**Require:** number of updates  $k$ , number of predictor steps  $P$ , number of corrector steps  $C$ .

- 1: Initialize time  $t \leftarrow 1$
  - 2: Initialize sample  $x \leftarrow \text{MASK}^D$
  - 3: Set predictor step size  $\Delta t \leftarrow (t - t_{min})/P$
  - 4: **for** step = 1 to  $P$  **do**
  - 5: Compute denoising probability  $p[d, i] = f^\theta(x)[d, i]$
  - 6: Apply predictor step  $x \leftarrow \text{PREDICTORUPDATE}(x, p, t)$
  - 7: Update time  $t \leftarrow t - \Delta t$
  - 8: **if**  $t > t_c$  **then**
  - 9: **Continue**
  - 8: **end if**
  - 10: **end if**
  - 11: **for**  $cstep = 1$  to  $C$  **do**
  - 12: Compute confidence score  $c[d] = \log p_{0|t}^\theta(x^d | x^{\setminus d}), \forall d \notin \mathcal{M}(x)$
  - 13: Sample Gumbel noise  $g[d] \sim \text{Gumbel}(0, 1)$
  - 14: Compute ranking criterion  $r[d] = -c[d] + \tau g[d]$
  - 15: // Update the top-k dimensions
  - 16: **for**  $cnt = 1$  to  $k$  **do**
  - 17: Get dimension of transition  $d^* = \text{SORTED}(r)[D - cnt]$
  - 18: Update state  $x^{d^*} \leftarrow \text{Categorical}(p_{0|t}^\theta(x^{d^*} | x^{\setminus d^*}))$
  - 19: **end for**
  - 20: **end for**
  - 21: **end for**
  - 22: // Deterministic update at the last step
  - 23: Find most likely values for each dimension given the rest  $x \leftarrow \text{argmax}_{x_0} p_{0|t}^\theta(x_0 | x)$
  - 24: **Return**  $x$
-

## C. Hollow Transformer Architecture

### C.1. Hollow Transformer Architecture Details

We build upon the hollow transformer in (Sun et al., 2022) and design a class of hollow transformers that is more parameter efficient and expressive. First, we divide the computation into two streams, the content (causal) stream and the query (mixing) stream. The content stream consists of two transformers with causal self-attention in opposite directions, whereas the query stream attend to the content stream and outputs the final result. By design, non of the attention mechanisms allow a token at position  $d$  to attend to a token that has access to information of  $x^d$ .

We differ from the original hollow transformer in that we introduce a third stream to combine information of the forward/backward causal streams. Specifically, we have the attention layers  $F_l$ ,  $B_l$ ,  $M_k$  that implement multi-head attention with different causal structures. The updates of these attention streams are respectively (ignoring multilayer perceptron layers):

$$F_{l+1}^d \leftarrow \text{Attention}(Q = F_l^d, KV = F_l^{\leq d}), \quad (54)$$

$$B_{l+1}^d \leftarrow \text{Attention}(Q = B_l^d, KV = B_l^{\geq d}), \quad (55)$$

$$M_{k+1}^d \leftarrow \text{Attention}(Q = h(M_k^d, F_{km}^d, B_{km}^d), KV = (F_{km}^{\leq d}, B_{km}^{\geq d})), \quad (56)$$

where we insert a mixing layer for every  $m$  forward/backward layers. Notably, the new mixing layer  $M_k$  acts like a ‘‘query stream’’ while the forward and backward layers  $F_l$  and  $B_l$  act like ‘‘content streams’’ (Yang, 2019). To prevent information leak and preserve the ‘‘hollowness,’’ we offset the inputs by one position when initializing the forward/backward layers:

$$F_1^d = \text{Embed}(\text{Pad}(x^{d-1})), B_1^d = \text{Embed}(\text{Pad}(x^{d+1})), \quad (57)$$

and we initialize the mixing layer to zero. Due to the attention structure, each position  $M^d$  of the mixing layer can have access to all the other positions  $x^{\setminus d}$  in the input  $x$ , and therefore it cannot attend to itself at other positions to preserve hollowness. We double the feature dimension of the mixing layer and set the update function  $h$  to:

$$h(M_k^d, F_{km}^d, B_{km}^d) = M_k^d + \text{Concat}(F_{km}^d, B_{km}^d). \quad (58)$$

Finally, we use the output from the last mixing layer to compute the output logits.

**Weight tying.** Since the forward and backward content streams carry out the same type of computation, we use a weight-tied network where all weights are shared between  $F_l$  and  $B_l$ , which significantly decreases the parameter count of our network and makes training and evaluation faster. In practice, we have not observed significant downgrade in performance of the weight-tied network on ImageNet.

## D. Experiments

The main experiments in this paper are performed on a v3-128 TPU pod and a v3-8 TPU machine with Google cloud.

### D.1. Hidden Markov Modeling

#### D.1.1. HYPERPARAMETER SELECTION

We select the hyperparameters for the correctors in the Markov chain experiments with grid search. For the informed corrector, the number of parallel updates  $k$  is swept over the values  $\{1, 2, 4, 8, 16\}$ , and the temperature hyperparameter is swept over  $\{0.01, .1, .5, 1., 2., 4.\}$ . For the uninformed corrector, the corrector step size is swept over  $\{0.01, 0.1, 0.5, 1.0, 1.5, 2.0, 3.0, 4.0, 5.0\}$ .

### D.2. Tokenized ImageNet

#### D.2.1. TRAINING DETAILS

Our model is adapted from that proposed by Sun et al. (2022) and consists of 24 standard transformer layers. We use an embedding dimension of 784 and hidden dimension of 2048. We add 3 mixture layers (1 after every 8 transformer layers) to the model to facilitate information exchange between the forward and backward streams. We train the model using

AdamW (Loshchilov & Hutter, 2019) with an initial learning rate of  $1e-4$  and a batch size of 512. We use a linear learning rate warmup in the first 100 steps. We adopt a stepwise learning rate schedule, dropping the learning rate to  $3.3e-5$  at  $2.11 \times 10^6$  steps and to  $1e-5$  at  $2.4 \times 10^6$  steps. We stop the training at  $2.5 \times 10^6$  steps.

### D.2.2. HYPERPARAMETER SELECTION

We select the hyperparameters for the samplers in the ImageNet experiments with grid search. For the informed corrector, the number of parallel updates  $k$  is swept over the values  $\{1, 2, 4, 8, 16\}$ , and the temperature hyperparameter is swept over  $\{.1, 1., 2., 10., 1000.\}$ . For the uninformed corrector, the corrector step size is swept over  $\{.5, 1., 2., 4.\}$ . For maskgit, the temperature hyperparameter is swept over  $\{0.5, 1., 2., 4., 8., 10., 12., 16., 20., 40.\}$ .

### D.2.3. ADDITIONAL EXAMPLE GENERATIONS

See Figures 6 to 8.

## E. Additional results

The additional experiments on the Text8 dataset were performed on a machine with 8 NVIDIA H100 GPUs .

### E.1. Text8

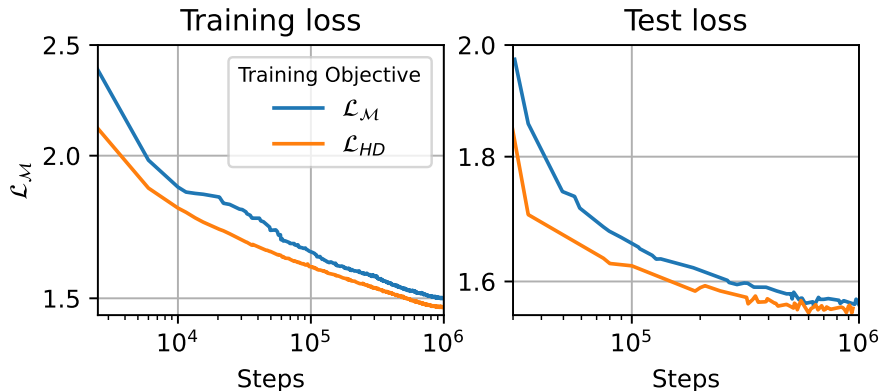


Figure 5: Loss curve on Text8 dataset (Mahoney, 2006)

We followed the standard dataset split and trained our models on text chunks of length 256 for 1 million steps with batch size 512. We train two models: one with the masked loss  $\mathcal{L}_M$  and the other with HollowDiff loss  $\mathcal{L}_{HD}$  on the text8 dataset of Mahoney (2006). The model consists of 12 standard transformer layers, and we add one mixing layer at the end to combine the forward and backward streams. We empirically confirmed that the model trained with our proposed HollowDiff loss function  $\mathcal{L}_{HD}$  is more efficient (see Figure 5).



Figure 6: Example informed corrector generations for the classes Pomeranian (259) and jack-o'-lantern (607).

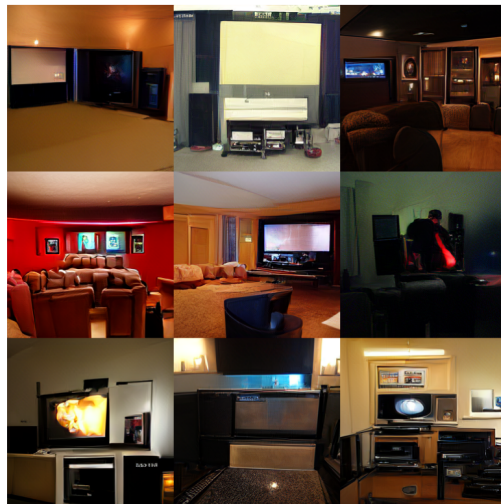


Figure 7: Example informed corrector generations for the classes timber wolf (269) and home theater (598).

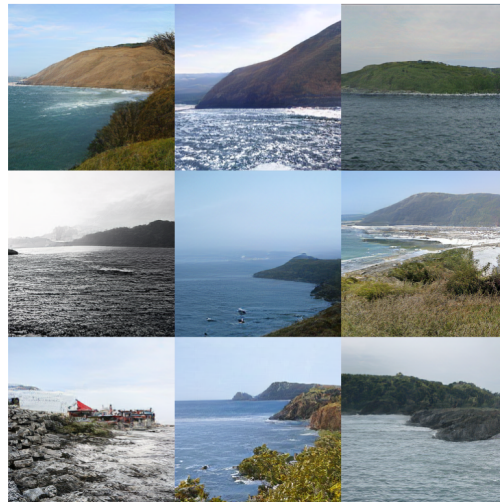


Figure 8: Example informed corrector generations for the classes seashore (978) and bolete (997).